

Ceramide Drives Cholesterol Out of the Ordered Lipid Bilayer Phase into the Crystal Phase in 1-Palmitoyl-2-oleoyl-*sn*-glycero-3-phosphocholine/Cholesterol/Ceramide Ternary Mixtures[†]

Md Rejwan Ali, Kwan Hon Cheng, and Juyang Huang*

Department of Physics, Texas Tech University, Lubbock, Texas 79409

Received March 28, 2006; Revised Manuscript Received August 9, 2006

ABSTRACT: The effect of brain ceramide on the maximum solubility of cholesterol in ternary mixtures of 1-palmitoyl-2-oleoyl-*sn*-glycero-3-phosphocholine (POPC), cholesterol, and ceramide was investigated at 37 °C by a cholesterol oxidase (COD) reaction rate assay and by optical microscopy. The COD reaction rate assay showed a sharp increase in cholesterol chemical potential as the cholesterol mole fraction approaches the solubility limit. A decline in the COD reaction rate was found after the formation of cholesterol crystals. The maximum solubility of brain ceramide in POPC bilayers was determined to be 68 ± 2 mol % by microscopy. We found that ceramide has a much higher affinity for the ordered bilayers than cholesterol, and the maximum solubility of cholesterol decreases with the increase in ceramide content. More significantly, the displacement of cholesterol by ceramide follows a 1:1 relation. At the cholesterol solubility limit, adding one more ceramide molecule to the lipid bilayer drives one cholesterol out of the bilayer into the cholesterol crystal phase, and cholesterol is incapable of displacing ceramide from the bilayer phase. On the basis of these findings, a ternary phase diagram of the POPC/cholesterol/ceramide mixture was constructed. The behaviors of ceramide and cholesterol can be explained by the umbrella model. Both ceramide and cholesterol have small polar headgroups and relatively large nonpolar bodies. In a PC bilayer, ceramide and cholesterol compete for the coverage of the headgroups of neighboring PC to prevent the exposure of their nonpolar bodies to water. This competition results in the 1:1 displacement as well as the displacement of cholesterol by ceramide from lipid raft domains.

Sphingomyelin and cholesterol represent the major components of lipid rafts in the plasma membranes of most animal cells. These raft domains are thought to be involved in regulating many important cell functions, such as signal transduction, lipid trafficking, and protein functions (1–3). Ceramide is an important lipid involved in many vital cell signaling processes (4, 5). It also plays a key role in many biochemical processes associated with cell proliferation, cell differentiation, and apoptosis (6, 7). In cells, ceramide can be generated by either *de novo* synthesis or the hydrolysis of sphingomyelins by acid sphingomyelinase (aSMase) or neutral sphingomyelinase (nSMase) during cellular stress and apoptosis (8–10). In lipid membranes, ceramide increases the acyl chain packing order and stabilizes the gel phase (11). Recently, the interaction between cholesterol and ceramide in cell membranes has drawn a lot of attention (12, 13). It has been shown that ceramide preferentially partitions into

lipid raft domains and displaces cholesterol from lipid rafts (14–16). However, cholesterol–ceramide interaction in a PC¹ lipid bilayer containing a high level of cholesterol or ceramide, as well as the phase diagram of the ternary mixtures, has not yet been investigated.

Previously, we have measured the solubility limit of cholesterol in lipid membranes (17). Above this limit, cholesterol precipitates from the bilayer to form cholesterol monohydrate crystals. Experiments with a careful sample preparation procedure yielded reproducible and precise cholesterol solubility limits: 66 ± 1 mol % for phosphatidylcholine (PC) bilayers and 51 ± 1 mol % for phosphatidylethanolamine (PE) bilayers (17). These data were further analyzed using Monte Carlo simulations in exploring the molecular interactions between phospholipids and cholesterol. We found that at high cholesterol concentrations, the dominant effects arise from a hydrophobic interaction, which is explained by the “umbrella model”. Cholesterol has a large nonpolar steroid ring body and a relatively small polar hydroxyl headgroup. In a bilayer, cholesterol relies on the coverage of polar headgroups of the neighboring phospholipid to prevent the unfavorable free energy of exposure of the nonpolar body part to water. As the cholesterol concentration increases, fewer lateral distributions of lipids can satisfy the coverage requirement. When the concentration of cholesterol increases to a point at which large clusters of cholesterol begin to form and not all of them can be

[†] This work was supported by the National Science Foundation (MCB-0344463), the Petroleum Research Fund (ACS PRF#41300-AC6), and the Welch Research Foundation (D-1158).

* To whom correspondence should be addressed. E-mail: juyang.huang@ttu.edu. Phone: (806) 742-4780. Fax: (806) 742-1182.

¹ Abbreviations: PC, phosphatidylcholine; POPC, 1-palmitoyl-2-oleoyl-*sn*-glycero-3-phosphocholine; PE, phosphatidylethanolamine; RSE, rapid solvent exchange method; COD, cholesterol oxidase; POD, peroxidase; χ_{chol} , cholesterol mole fraction; χ^* , cholesterol maximum solubility in a lipid bilayer; χ_{cer} , ceramide mole fraction; rhodamine-PE, 1,2-dioleoyl-*sn*-glycero-3-phosphoethanolamine-*n*-(lissamine rhodamine B sulfonyl).

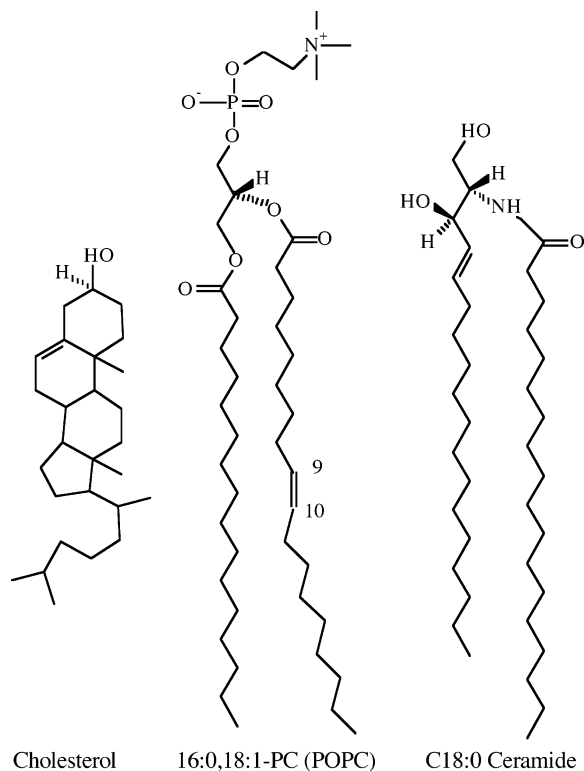


FIGURE 1: Chemical structures of cholesterol, POPC, and the main component of brain ceramide (C18:0 ceramide). Both cholesterol and ceramide have small polar headgroups and relatively large nonpolar bodies. POPC has a much larger polar headgroup.

effectively covered by phospholipid headgroups, the cholesterol chemical potential jumps sharply and leads to the precipitation of cholesterol from the bilayer. The phenomenon of cholesterol precipitation most likely occurs near three discrete cholesterol mole fractions of 0.50, 0.57, and 0.67, which correspond to cholesterol:phospholipid molar ratios of 1:1, 4:3, and 2:1, respectively. At these solubility limits, the cholesterol/phospholipid bilayer mixture forms highly regular lipid distributions to minimize cholesterol–cholesterol contacts (18, 19).

Although the molecular structure of ceramide is quite different from that of cholesterol as shown in Figure 1, both molecules have a small polar headgroup and a large nonpolar body. On the basis of the umbrella model as discussed above, it is likely that ceramide in a lipid bilayer also needs the coverage of the neighboring PC headgroups to shield its nonpolar body from water exposure like cholesterol does. This is consistent with recent reports that ceramide displaces cholesterol from lipid raft domains (14–16). London and London (14) suggested that ceramide and cholesterol both compete for the association with the lipid rafts because of a limited capacity of raft lipids with large headgroups to accommodate small headgroup lipids. If the behavior of ceramide in a lipid bilayer can also be described by the umbrella model, one would expect that this competition between cholesterol and ceramide could affect the maximum solubility of cholesterol in the lipid bilayer. Since ceramide competes with cholesterol for the coverage of neighboring PC headgroups, the more ceramide is present in a PC bilayer, the less the bilayers can accommodate cholesterol. In other words, one expects a consistent decline of the value of the cholesterol solubility limit in response to an increasing ceramide content in the lipid bilayers.

In this study, the effect of ceramide on the maximum solubility of cholesterol (χ^*) in ternary lipid mixtures of POPC, cholesterol, and ceramide was investigated systematically. A bilayer surface sensitive technique, the cholesterol oxidase (COD) reaction rate assay, has been developed to measure χ^* . We found that the value of the maximum solubility limit of cholesterol indeed decreases concomitantly with the increase in ceramide concentration, as predicted by the umbrella model. Most significantly, we found that ceramide has a much higher affinity for the lipid bilayer phase than cholesterol does. One ceramide molecule displaces one cholesterol from the bilayer phase into the cholesterol crystal phase at the solubility limit, and cholesterol is incapable of displacing ceramide from the lipid bilayer. This 1:1 relationship allowed us to construct a phase diagram of POPC/cholesterol/ceramide mixtures, which describes the crystal and bilayer phases in this ternary system.

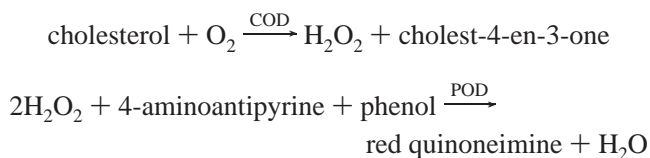
MATERIALS AND METHODS

Materials. POPC, brain ceramide, and rhodamine-PE were purchased from Avanti Polar Lipids, Inc. (Alabaster, AL). The typical fatty acid distribution for brain ceramide is as follows: 58% C18:0, 15% C24:1, 9% C22:0, 7% C24:0, 6% C20:0, 2% C16:0, and 3% others (20). Cholesterol was purchased from Nu Chek Prep, Inc. (Elysian, MN). Lipid purity (>99%) was confirmed by thin layer chromatography (TLC) on washed, activated silica gel plates (Alltech Associates, Inc., Deerfield, IL) and developed with a 65:25:4 chloroform/methanol/water mixture for phospholipid analysis or with a 7:3:3 petroleum ether/ethyl ether/chloroform mixture for cholesterol analysis. The TLC plates were visualized by being heated on a 200 °C hotplate for 2 h after being sprayed with a 20% ammonium sulfate solution. All solvents were HPLC grade. Concentrations of phospholipid stock solutions were determined with a phosphate assay (21). Aqueous buffer [5 mM PIPES, 200 mM KCl, and 1 mM NaN₃ (pH 7.0)] was prepared from deionized water (~18 M Ω) and filtered through a 0.1 μ m filter before use. Recombinant cholesterol oxidase expressed in *Escherichia coli* (C-1235), peroxidase (P-8250) from horseradish, and other chemicals for the cholesterol oxidation measurements were obtained from Sigma (St. Louis, MO).

Liposome Preparation. The cholesterol content in all samples was kept at 60 μ g, and the lipid compositions of samples were adjusted by adding appropriate amounts of POPC and ceramide. For microscopy experiments, lipid mixtures were also labeled with 0.5% rhodamine-PE. Liposomes were prepared by the rapid solvent exchange (RSE) method (22). First, lipids were dissolved in 70 μ L of chloroform. The lipid solution was then heated to 55 °C briefly in a glass tube, and 1.3 mL of aqueous buffer was added. While the mixture was kept vigorously vortexed in the glass tube, the bulk solvent was removed by gradually reducing the pressure to ~3 cm of Hg using a home-built vacuum attachment. The remaining trace chloroform was removed by vortexing for an additional 1 min at the same pressure. The liposomes prepared by these procedures were all sealed under argon. The samples were then placed in a programmable water bath (VWR, model 1187P), preheated to 50 °C for the subsequent heating and cooling cycle. The samples were first cooled to 24 °C at a rate of 10 °C/h and again heated to 50 °C at the same rate. The samples were

then kept at 50 °C for an additional 1 h before finally being cooled to room temperature at a rate of 1.5 °C/h. Finally, the liposomes were stored at room temperature on a mechanical shaker for ~10 days in the dark before the cholesterol oxidation measurements.

Cholesterol Oxidation Measurements. Cholesterol oxidase (COD) is a water-soluble monomeric enzyme that catalyzes the conversion of cholesterol to cholest-4-en-3-one. The initial rate of oxidation of cholesterol by the oxidase enzyme was determined through a coupled enzyme assay scheme as shown below.



The total reaction involves two steps. In the first step, the COD-mediated oxidation of membrane cholesterol produces two products, hydrogen peroxide and cholest-4-en-3-one (23). Catalyzed by peroxidase (POD), the production of hydrogen peroxide in the first step subsequently leads to reaction with 4-aminoantipyrine and phenol and produces red-colored quinoneimine, which has a distinctive absorption peak at 500 nm (24). For each cholesterol oxidation measurement, 1.3 mL of liposomes was first mixed with 0.2 mL of a 140 mM phenol solution. After mixing had been carried out, 1 mL of reaction buffer [1.64 mM aminoantipyrine and 10 units/mL peroxidase in PBS buffer (pH 7.40)] was added. The above mixture was then incubated at 37 °C for at least 10 min and finally transferred to a cuvette preheated to 37 °C in a heating block. The sample in the cuvette was maintained at 37 °C and stirred with a home-built magnetic mini-stirrer during the measurement. An HP-8453 (UV–vis) linear diode array spectrophotometer (Agilent Technologies, Wilmington, DE) was used to measure the absorption spectra of the samples. The reaction was started by injecting 20 μL of a COD solution (5 units/mL) into the cuvette. The time-resolved absorption spectra (190–1100 nm) were collected with an integration time of 0.5 s. The spectra were collected at a rate of two spectra per second, and the total data collection time per sample was 120 s. Background-corrected time-dependent absorption of quinoneimine was determined by calculating the difference in the absorption at 500 nm and the background average over the range of 700–800 nm as a function of time. The initial oxidation rate, i.e., the rate of change in the quinoneimine absorption at time zero, was determined using a second-order polynomial fit to the first 40 s of the absorption data. All data acquisition and data analysis were performed using the UV–visible ChemStation Software provided by Agilent Technologies. For all experiments, each sample contained the same amount of cholesterol (60 μg). This ensured that the bulk concentration of available substrate to COD remained constant.

Optical and Fluorescence Microscopy. Optical microscopy was used to determine the solubility limit of ceramide in POPC bilayers and to confirm the presence of crystal and bilayer phases in POPC/ceramide/cholesterol ternary mixtures. The detailed methodology for optical microscopy has been described in a previous paper (17). Fluorescence microscopy was also used to visualize lipid vesicles, since

rhodamine-PE is very effective in labeling lipid vesicles, but not cholesterol crystals or ceramide crystals. An Olympus (Melville, NY) IX70 inverted microscope was used in the Nomarski differential interference contrast (Nomarski DIC) mode. A 20 \times air (UplanFl) or a 60 \times water immersion (UplanApo) objective manufactured by Olympus was used. Digital images were captured by a Cooke (Auburn Hills, MI) SensiCam CCD camera. Lipid dispersions made by the RSE method were first concentrated with a tabletop centrifuge and viewed on thin cover glasses. For the determination of the maximum solubility of ceramide in the POPC bilayer, a series of POPC/ceramide mixtures with increasing ceramide mole fractions were examined, and the critical mole fraction above which ceramide crystals were present was determined. For POPC/ceramide/cholesterol ternary samples, the presence of crystal phases was determined by visual inspection, and the type of the crystal, ceramide or cholesterol, was further identified by the crystal shape.

RESULTS

Maximum Solubility of Ceramide in POPC Bilayers. The maximum solubility of brain ceramide in POPC bilayers was measured by optical microscopy. No ceramide crystals were found on samples with a ceramide mole fraction of <0.66. Above the critical mole fraction of 0.68, ceramide crystals were consistently detected in the samples. Fluorescence microscopy was also used to visualize the lipid vesicles, which exhibited a bright fluorescence from the rhodamine-PE label. Unlike cholesterol monohydrate crystals, which exhibit a sharp-edged planar shape, the ceramide crystals are often quite irregular in shape. On the basis of the microscopic measurements from three independent sets of ceramide/POPC binary mixtures, the maximum solubility of ceramide in POPC bilayer was determined to be 0.68 ± 0.02 . It is interesting to note that the maximum solubility of brain ceramide in POPC bilayers is similar to the maximum solubility of cholesterol in POPC bilayers. Previously, we found that χ^* is 0.66 ± 0.01 for many PCs with the acyl chain length ranging from 12 to 22 carbons (17). We believe that χ^* is not sensitive to the acyl chain length, because chain length makes little difference to the coverage requirement (18). Although brain ceramide is not a pure substance as it is composed of a number of long chain ceramides (see Materials and Methods), we expect that these long chain ceramides have the same solubility limit in POPC bilayers, which is independent of their chain lengths.

COD Reaction Rate Assay. In this study, we developed a new COD reaction rate assay for determining the maximum solubility of cholesterol (χ^*) in a lipid bilayer. Previously, χ^* has been measured by various other techniques, such as X-ray diffraction, light scattering, microscopy, and differential scanning calorimetry (17, 25, 26). This new COD reaction rate assay is more convenient and has a higher resolution than the techniques mentioned above. We first used POPC for our calibration, since it has been well-established that the χ^* in POPC is 0.66 ± 0.01 (17).

It has been shown that a COD enzyme first physically associates itself with lipid bilayers without perturbing the membrane structure (23). The enzyme then goes through conformation changes and provides a hydrophobic binding cavity that allows a favorable partitioning of the cholesterol

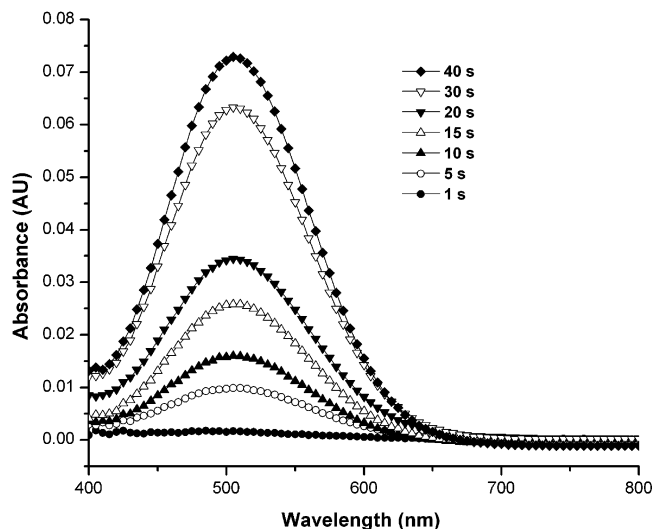


FIGURE 2: Absorption spectra of a POPC/cholesterol mixture with a χ_{chol} of 0.60, at several time points after the injection of COD enzyme. The absorption peak at 500 nm is from red quinoneimine, one of the final products of the coupled enzyme reactions.

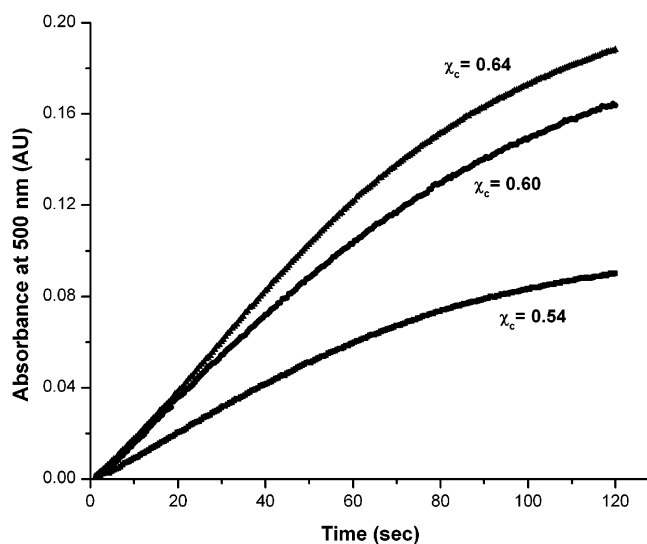


FIGURE 3: Absorption at 500 nm as a function of time for three POPC/cholesterol binary mixtures. The first 40 s of data for each sample was used to fit a second-order reaction curve and to calculate the initial reaction rate.

from the membrane into the COD cavity. The reaction rate of the oxidation sensitively depends on the cholesterol concentration (i.e., substrate concentration) and the cholesterol chemical potential (i.e., inherent stability of cholesterol) in a lipid bilayer (23), which is directly related to the cholesterol lateral organization within the bilayer (27). Since the cholesterol content in our samples was a constant, the initial reaction rate of COD essentially reflects the chemical potential of cholesterol in lipid bilayers, assuming that all the cholesterol remains in the bilayer phase. Figure 2 shows the representative absorption spectra of a POPC/cholesterol binary mixture with a χ_{chol} of 0.60 at various time points, after the injection of the COD enzyme. The height of the absorption peak of the COD assay product, red quinoneimine (see Materials and Methods), at 500 nm was found to increase steadily with time, indicating the progress of the COD-mediated cholesterol oxidation reaction. Figure 3 shows the absorption at 500 nm versus time for three POPC/cholesterol mixtures: $\chi_{\text{chol}} = 0.54, 0.60,$ and 0.64 . Because

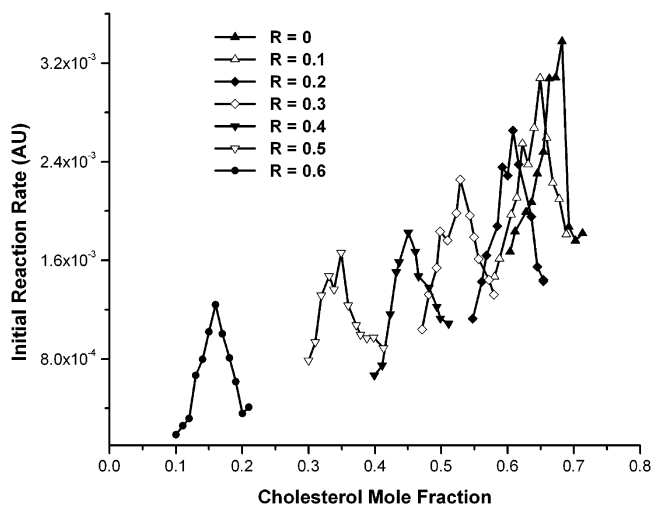


FIGURE 4: Initial reaction rates as a function of cholesterol mole fraction for seven sets of POPC/cholesterol/ceramide mixtures. Each set has a predetermined R ratio, where $R = \text{ceramide}/(\text{ceramide} + \text{POPC})$. The peak location of each curve indicates the maximum solubility of cholesterol in lipid bilayers with that particular R .

of the concern that the accumulation of the oxidized cholesterol product (i.e., cholest-4-en-3-one) in the lipid bilayer may alter the membrane properties (23, 27), only the first 40 s of data was used to fit a second-order polynomial and to calculate the initial rate (i.e., initial slope) of the reaction. It is interesting to notice that Ahn and Sampson have observed sigmoidal reaction progress curves over the time scale ranging from 20 to 200 min, primarily due to the increasing COD catalytic rate constant caused by the accumulation of the oxidized cholesterol product (i.e., cholest-4-en-3-one) in the lipid bilayers (23). In this study, since the measurements were taken over a much shorter time period and much less cholest-4-en-3-one was produced, the reaction progress curves were essentially hyperbolic. On the basis of the absorption readings at 500 nm taken 2 h after the injection of the COD enzyme, we estimated that $\sim 1\text{--}10\%$ of the cholesterol-oxidized product was formed during the first 40 s of the reaction, depending on the actual reaction rate. As shown in Figure 3, the initial rate increases with the cholesterol mole fraction. This increase is not a surprise. Previously, on the basis of thermodynamic analysis and Monte Carlo simulation, we predicted that the chemical potential of cholesterol in a lipid bilayer should increase sharply near its solubility limit, to approach that in cholesterol monohydrate crystals (see Figure 4e in ref 18). In a previous study, Ahn and Sampson also observed that the chemical potential of cholesterol increases with the mole fraction of cholesterol at low cholesterol concentrations (23).

Figure 4 shows the initial rate of COD reaction as a function of cholesterol mole fraction for seven sets of POPC/ceramide/cholesterol mixtures. Here, the molar ratio R is defined as $\text{ceramide}/(\text{ceramide} + \text{POPC})$. For the $R = 0$ curve, there is no ceramide, and the mixtures are POPC/cholesterol binary mixtures. This curve peaks at a χ_{chol} of 0.67, which agrees with the maximum solubility of cholesterol in POPC bilayers (17). The increase in the COD initial reaction rate with an increase in cholesterol content for a cholesterol mole fraction < 0.67 should be primarily due to the increase in the chemical potential of cholesterol. However, why does the COD initial reaction rate drop when the

overall cholesterol mole fraction is above χ^* ? Two important factors that affect the COD reaction rate are the amount of bilayer cholesterol accessible to the COD enzyme and the chemical potential of cholesterol. The drop cannot be due to the change in cholesterol chemical potential, since above χ^* , the bilayer phase is in thermodynamic equilibrium with the cholesterol crystal phase and the chemical potential of cholesterol should become a constant. However, the amount of bilayer cholesterol in a sample accessible to the COD enzyme decreases above χ^* . Since every sample has an identical amount of cholesterol (60 μg), when the overall cholesterol mole fraction of a sample is above χ^* , some cholesterol will be in the cholesterol crystal phase, and less cholesterol will remain in the bilayer phase. Thus, the effective substrate (i.e., the bilayer cholesterol) concentration decreases above χ^* . Other mechanisms may also contribute to the drop. For example, cholesterol microcrystals could physically change the packing order of lipids and the curvature of lipid bilayers and affect COD activity. In previous X-ray diffraction experiments, it has been found that as soon as the cholesterol mole fraction passes the solubility limit and cholesterol monohydrate crystals begin to form, the broad wide-angle diffraction peak at 4.9 \AA , corresponding to the acyl chain packing in the bilayers, quickly disappears (17).

The second part of the coupled enzyme assay adapted in this study involves using phenol and 4-aminoantipyrine (see Materials and Methods). To investigate the effect of these chemicals on bilayer structure and the chemical potential of cholesterol, a control experiment in which the second part of the coupled enzyme assay was removed and the production of cholest-4-en-3-one was directly monitored by measuring its absorption peak at 240 nm was carried out as described by Ahn and Sampson (23). We found that the initial reaction rates obtained from the control experiment (data not shown) had essentially the same composition dependence and peak locations as those obtained from the coupled enzyme assay shown in Figure 4. Thus, it appeared that phenol and 4-aminoantipyrine did not cause a detectable change in the bilayer structure or chemical potential of cholesterol.

The fact that the location of the peak in the COD initial reaction rate versus lipid composition plot coincides with the cholesterol solubility limit leads us to propose that this COD reaction peak detection assay can be a useful tool for measuring χ^* . Previously, χ^* in pure PC bilayers was determined to be ~ 0.67 by X-ray diffraction, light scattering, and optical microscopy (17, 25). The peak position in Figure 4 is in excellent agreement with all those previous measurements. We also tested this new assay with several other phosphatidylcholines, such as di14:0-PC (DMPC), di16:0-PC (DPPC), and di18:1-PC (DOPC). The χ^* values that were obtained (~ 0.67) were in excellent agreement with previous results as well (data not shown). Therefore, the sharp peak in the COD initial reaction rate versus cholesterol composition plot is a new and sensitive method for determining the cholesterol maximum solubility in lipid bilayers. It has been reported previously that the COD reaction rate peaks at several cholesterol mole fractions far below the solubility limit, due to the formation of cholesterol "superlattice" domains (27). These peaks likely originated from different mechanisms and do not involve the formation of the cholesterol crystal phase.

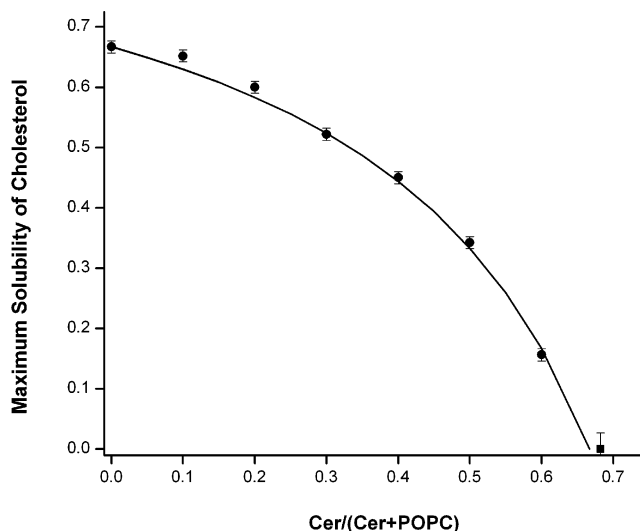


FIGURE 5: Maximum solubility of cholesterol, χ^* , as a function of ceramide/(ceramide + POPC) ratio: (●) χ^* values obtained from three independent COD reaction rate measurements and (■) maximum solubility of ceramide in POPC bilayers determined by optical microscopy. The solid line is the theoretical χ^* curve given by eq 3, with the assumption that one ceramide molecule displaces one cholesterol from the bilayer phase into the cholesterol crystal phase.

Maximum Solubility of Cholesterol in POPC/Cholesterol/Ceramide Ternary Mixtures. Figure 4 also shows the COD initial reaction rate as a function of cholesterol mole fraction at six other R ratios. For each set of experiments, R was kept constant for all samples. For each R value, there is a clear global peak in the COD initial reaction rate, which indicates the cholesterol maximum solubility in the lipid bilayers with that particular R . Clearly, the higher the ceramide concentration, the lower the cholesterol maximum solubility. Figure 5 shows the cholesterol maximum solubility as a function of R . The filled circles are averaged χ^* values determined from three independent COD reaction rate experiments. The filled square is the ceramide maximum solubility in POPC bilayers determined by microscopy. The value of χ^* , starting from 0.67 in POPC, decreases with an increase in ceramide concentration and eventually becomes zero when $R = 0.68$. The results strongly suggest that cholesterol is displaced by ceramide from the bilayer phase into the crystal phase. The more ceramide is present in a bilayer, the less the bilayer can accommodate cholesterol. Most significantly, our data also suggest that each ceramide molecule displaces one cholesterol molecule from the bilayer phase. To test this hypothesis over the entire range of R values, we calculated the theoretical value of χ^* as a function of R with this 1:1 displacement assumption. Let χ_{PC}^* be the maximum solubility of cholesterol in POPC bilayers and define χ^* in POPC/cholesterol/ceramide ternary mixtures as

$$\chi^* = \text{chol}/(\text{chol} + \text{POPC} + \text{cer}) \quad (1)$$

at the cholesterol solubility limit. Assume that adding one ceramide molecule would displace one cholesterol molecule from the lipid bilayer phase, then at the solubility limit

$$(\text{cer} + \text{chol})/(\text{chol} + \text{POPC} + \text{cer}) = \chi_{\text{PC}}^* \quad (2)$$

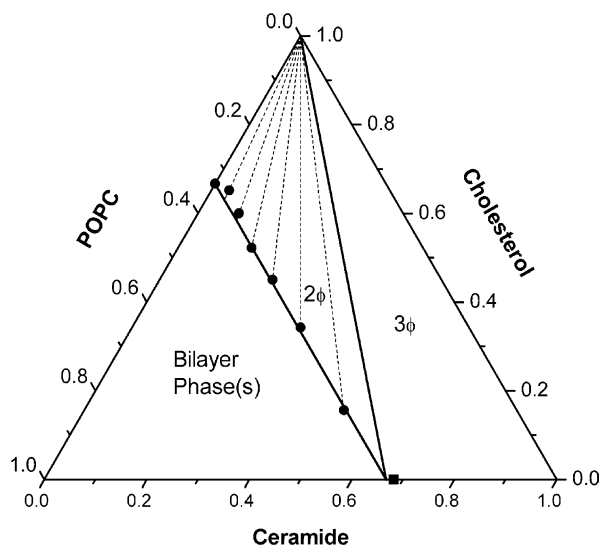


FIGURE 6: Ternary phase diagram of POPC/cholesterol/ceramide mixtures, along with the maximum solubility data: (●) χ^* values obtained from COD reaction rate measurements and (■) maximum solubility of ceramide in POPC bilayers determined by optical microscopy. In the bilayer phase(s) region, all POPC, cholesterol, and ceramide molecules are in the lipid bilayer(s). In the two-phase (2ϕ) region, the bilayer phase coexists with cholesterol monohydrate crystals. The dashed lines are thermodynamic tie lines, which indicate the compositions and amounts of two coexisting phases. In the three-phase (3ϕ) region, the lipid bilayer phase containing all POPC molecules and 67 mole % brain ceramide coexists with cholesterol monohydrate crystals and ceramide crystals.

Solving eqs 1 and 2 together, we obtained the theoretical prediction of χ^* as a function of R as shown below.

$$\chi^*(\text{theory}) = (\chi_{PC}^* - R)/(1 - R) \quad (3)$$

The solid line in Figure 5 is the theoretical χ^* curve given by eq 3. It is clear from Figure 5 that there is a very good agreement between the theoretical curve and the experimental data over the entire range of R values. This confirms that the displacement of cholesterol by ceramide from the bilayer phase to the cholesterol crystal phase is indeed 1:1. Ceramide has a much higher affinity for the ordered bilayer phase than cholesterol, and cholesterol cannot displace ceramide from the lipid bilayer phase.

POPC/Cholesterol/Ceramide Ternary Phase Diagram. A POPC/cholesterol/ceramide ternary phase diagram was subsequently constructed on the basis of our COD initial reaction rate and microscopy data and is shown in Figure 6. Interestingly, our χ^* data points at various R ratios form a straight line ($\chi_{chol} + \chi_{cer} = 0.67$) in the ternary phase diagram. This observed straight line provides evidence that supports the hypothesis that the displacement of cholesterol by ceramide is a 1:1 process. As shown in Figure 6, the bilayer phase region is bounded by the boundary $\chi_{chol} + \chi_{cer} \leq 0.67$. In this region, all lipid molecules are in the bilayer phase(s), and no crystal of any kind exists. It has been reported that multiple bilayer phases can coexist in this region (28), but our experiments were not designed to investigate this question. In the two-phase region (labeled 2ϕ), the lipid bilayer phase and the cholesterol monohydrate crystal phase coexist. The region is bounded by two boundaries: $\chi_{chol} + \chi_{cer} \geq 0.67$ and $\chi_{cer} \leq 0.67$. In this region, the bilayer phase contains all the POPC and all ceramide molecules, as well

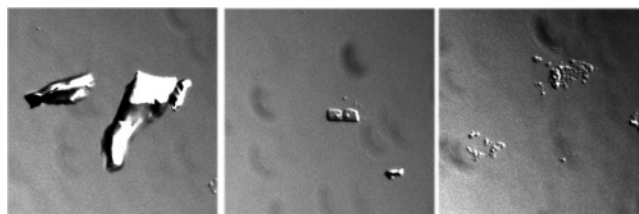


FIGURE 7: Nomarski DIC images taken from a POPC/cholesterol/ceramide mixture in the three-phase region, with a 15:35.8:49.2 POPC:cholesterol:ceramide composition: (left) ceramide crystals, (middle) cholesterol crystals, and (right) vesicles. Ceramide crystals are usually large in size and irregular in shape. Cholesterol crystals have a typical planar shape with sharp edges. Images show three phases coexisting in this mixture.

as the maximum amount of cholesterol that can be accommodated by the bilayer. Excess cholesterol will form cholesterol monohydrate crystals. Note that optical microscopy confirmed the coexistence of lipid vesicles and cholesterol crystals, and no ceramide crystal was observed in this region. The dashed lines are thermodynamic tie lines that indicate the compositions and amounts of coexisting phases. In the three-phase region (labeled 3ϕ), a bilayer phase, a cholesterol monohydrate crystal phase, and a ceramide crystal phase coexist. This region is bounded by one boundary: $\chi_{cer} \geq 0.67$. The three corners of the region specify the compositions of the three phases. The bilayer phase contains all the POPC molecules and the saturated amount of ceramide [i.e., bilayer ceramide/(bilayer ceramide + POPC) = 0.67]. No cholesterol is present in the lipid bilayer, since all cholesterol molecules have been displaced by ceramide. Excess ceramide forms ceramide crystals, and all cholesterol is in the form of cholesterol monohydrate crystals. To confirm the phases in the three-phase region, optical and fluorescence microscopy were used to examine mixtures in this region. Figure 7 shows three representative Nomarski DIC images taken from a POPC/cholesterol/ceramide ternary mixture in the three-phase region, with a 15:35.8:49.2 POPC:cholesterol:ceramide composition. This mixture contains ceramide crystals, cholesterol crystals, and vesicles. Vesicles made by the RSE method are usually small, compared with that made from the dry film method. Complementary rhodamine-PE fluorescence images were also obtained to confirm the bilayer phase (data not shown).

DISCUSSION

Sample Preparation Method. In this study, the RSE method was chosen to prepare POPC/cholesterol/ceramide mixtures for two main reasons. (i) The COD reaction rate measurement typically uses large unilamellar vesicles (LUVs), since the reaction rate depends on the membrane surface area accessible to COD enzymes. Large unilamellar vesicles can be made either by the extrusion method or by the ethanol injection method (29). The extrusion method is labor intensive, and the binding of lipids to polycarbonate membranes could be a real concern (27). In addition, samples with high cholesterol content often clog the filter membrane, and large crystals of cholesterol and ceramide simply cannot pass through the membrane. With the ethanol injection method, we found that the residue ethanol, which is typically ~1% of the total aqueous volume, significantly decreased the COD reaction rate, and the decrease was strongly dependent on the amount of ethanol in a sample. This effect

of ethanol on the COD reaction rate was not limited to liposomes made by the ethanol injection method. Adding ethanol to liposome samples made by the RSE method also resulted in a similar decrease. It is not clear whether ethanol causes the change in membrane structure or interferes with the COD oxidation process. We tested the ethanol injection method with a set of POPC/cholesterol samples and found that the data obtained were noisier and the COD reaction rates were lower than those with RSE samples (data not shown). However, the overall shape of the COD initial rate versus cholesterol mole fraction curve as well as its peak position was essentially identical to that from RSE samples shown in Figure 4, which indicated that the RSE method did not introduce a measurable composition-dependent change in COD accessible surface area. Compared with other methods, RSE is a convenient method with no binding or contamination concern. In addition, the accessible external surface in RSE samples is $\sim 33\%$ of the total lipids, which is quite close to the 50% theoretical value for true unilamellar vesicles (22). (ii) Measuring χ^* involves samples with a high mole fraction of cholesterol. Previously, we found that making a truly equilibrium phospholipid and cholesterol suspension is a quite challenging task. Some conventional sample preparation methods, such as the dry film or lyophilization from benzene, can induce cholesterol crystals in samples with a cholesterol mole fraction far below the true maximum solubility of cholesterol. Thus, samples made by these methods often yield a falsely low χ^* value as a result of sample preparation artifacts. Two sample preparation methods, low-temperature trapping (LTT) and rapid solvent exchange (RSE), were specifically developed to overcome this problem (17, 22). Samples made by either LTT or RSE method yield the true thermodynamic equilibrium χ^* value. Therefore, in this study, all samples were made by the RSE method.

The 1:1 Displacement. Our results established that a POPC bilayer could accommodate either up to 67 mol % cholesterol, 67 mol % ceramide, or a combined 67 mol % cholesterol and ceramide. The umbrella model gives a clear explanation about the mechanism of the 1:1 displacement. Previously, we interpreted χ^* in PC as the maximum amount of cholesterol that can be covered by the headgroups of PCs. Our Monte Carlo simulation showed that lipids form a highly ordered "maze pattern" lateral distribution in the bilayer at the solubility limit (18). Like cholesterol, ceramide molecules also have small polar headgroups and large nonpolar bodies. Neither cholesterol nor ceramide can form a bilayer by itself in water, since their small polar headgroups cannot protect their large nonpolar bodies from water. Thus, in water, both cholesterol and ceramide form crystals instead of bilayers. In a PC bilayer, ceramide competes with cholesterol for the coverage of PC headgroups. Since at the solubility limit, the "coverage capability" of PCs has been stretched to the limit, covering one additional ceramide is at the cost of covering one fewer cholesterol. This explains why all our χ^* data points form the straight line ($\chi_{\text{chol}} + \chi_{\text{cer}} = 0.67$) in Figure 6. The 1:1 displacement validates the umbrella model's physical interpretation of χ^* .

Why Ceramide Has a Much Higher Affinity for POPC than Cholesterol. Our data showed that ceramide has a much higher affinity for POPC bilayers than cholesterol, and cholesterol can be incorporated into a POPC bilayer only

after all ceramide molecules have been accommodated. In addition, at the solubility limit of cholesterol, ceramide displaces cholesterol from the bilayer phase into the cholesterol crystal phase. One possible reason contributing to the ceramide's high affinity is the fact that the long saturated chains of ceramide allow a tight packing of the acyl chains of PC around ceramide, which is more difficult with the sterol rings of cholesterol. London and London have shown that the tight lipid packing is important for the displacement of cholesterol (14). Another possible reason contributing to ceramide's high affinity is the fact that ceramide has a higher "headgroup:body" ratio than cholesterol. Cholesterol's polar headgroup has one hydroxyl, and the cross-sectional area of its nonpolar body is $\sim 37 \text{ \AA}^2$ (30). On the other hand, ceramide's polar headgroup has two hydroxyls, and the cross-sectional area of two long saturated acyl chains is only $\sim 40\text{--}42 \text{ \AA}^2$ (12, 31), not much larger than that of cholesterol. Thus, ceramide has a significantly higher headgroup:body ratio than cholesterol, although its polar headgroup is still not large enough to completely protect its nonpolar body from the exposure of water. On the basis of this consideration, it should be much easier for the neighboring PCs to cover ceramide than cholesterol, or equivalently, the free energy cost for covering ceramide should be much lower than that for covering cholesterol. Both mechanisms described above could contribute to a higher affinity of ceramide for the bilayer phase than cholesterol. One piece of experimental evidence that supports this explanation is the fact that the chemical potential of cholesterol decreases when some cholesterol is displaced by ceramide. In Figure 4, there is a general trend that the COD initial reaction rate, which is related to cholesterol chemical potential, decreases with the increase in R . Thus, the bilayer is more "relaxed" or at a lower free energy state when cholesterol is displaced by ceramide. Previous Monte Carlo simulations showed that at the maximum solubility limit, cholesterol adapts a maze lateral distribution pattern in POPC, which has a precise cholesterol:PC ratio of 2:1 or a χ^* value of 0.67. In a lipid bilayer composed of smaller headgroup lipids, such as POPE which is less capable of covering neighboring cholesterol than PC, cholesterol adapts a "hexagonal" lateral distribution pattern, which has a cholesterol:PE ratio of 1:1 or a χ^* value of 0.50 (18). The umbrella model together with the simulations showed that the change in the χ^* value is likely to be discontinuous in response to the change of headgroup:body ratio of host lipids. Some small changes in the headgroup:body ratio would not alter the χ^* value, but a sufficiently large change can cause membrane lipids to adapt a new lateral packing pattern and result in an abrupt change in χ^* . χ^* could jump from 0.50 (hexagonal pattern) to 0.57 ("dimer" pattern) and then to 0.67 (maze pattern), as the headgroup:body ratio increases continuously. The 1:1 replacement indicates that the lateral packing of ceramide with POPC is likely to be the same maze pattern, which suggests that the difference in the headgroup:body ratio of ceramide and cholesterol is not large enough for lipids to adapt a different lateral packing pattern to accommodate more ceramide.

Interaction of Ceramide with Lipid Rafts. The ceramide concentration on cell membranes can increase significantly through the action of sphingomyelinase, which converts sphingomyelins into ceramides. It has been shown in a

number of studies that ceramide has a strong affinity for the lipid raft domains, and ceramide displaces cholesterol from lipid raft domains (14–16). Raft domains are membrane domains with highly ordered acyl chains and rich in sphingomyelin and cholesterol. Raft domains coexist with liquid-disordered lipid domains, which are rich in PCs with unsaturated chains. Our result is consistent with other group's findings that ceramide competes with cholesterol for the coverage from large headgroup lipids, and ceramide has a higher affinity for large headgroup lipids than cholesterol. However, in the lipid raft system, the displacement of cholesterol by ceramide is not simply 1:1, and cholesterol can also displace ceramide from the lipid raft domains, to a certain extent (14). We should point out that an important difference is the fact that the cholesterol and ceramide concentrations in the raft studies were relatively low, compared to that in ours. Ceramide and cholesterol can redistribute themselves within the bilayers between the raft phase and the liquid-disordered phase, without involving any crystal phases. Thus, the displacement of cholesterol by ceramide from the raft domains is determined by the relative affinities of cholesterol and ceramide for the raft phase and the liquid-disordered phase. In our system, the competition between ceramide and cholesterol is for the only large headgroup lipids available in the bilayer, POPC. Although this study was conducted at high cholesterol and ceramide concentrations, we believe that the interesting molecular interactions it uncovered can help us to understand the behaviors of cholesterol and ceramide at other concentrations as well.

Umbrella Model. The umbrella model and the subsequent quantitative calculations based on the model have been successful in explaining and predicting a number of behaviors of cholesterol and ceramide in lipid membranes. (i) It successfully explained the χ^* value difference in PC and PE bilayers. PE has a smaller headgroup than PC. Therefore, PE can accommodate less cholesterol than PC. It also explained why the value of χ^* is not sensitive to the acyl chain length of the phospholipids. (ii) It explained the discrete value of χ^* . On the basis of our Monte Carlo simulations, cholesterol precipitation is most likely to occur at χ_{chol} values of 0.5, 0.57, and 0.67, where the chemical potential of cholesterol jumps (18). (iii) One interesting prediction from our Monte Carlo simulation studies was that there should be a cholesterol regular distribution (a hexagon pattern) at the cholesterol mole fraction of 0.50, a dimer pattern at 0.57, and a maze pattern at the saturation point, 0.67 (18). The regular distribution with a χ_{chol} of 0.57 had not been observed previously and was only predicted from our simulation based on the umbrella model. This prediction was confirmed in a DOPC/cholesterol system, using fluorescence anisotropy and fluorescence resonance energy transfer (FRET) measurements (25). In addition, the fluorescence lifetime of DPH-PC also exhibited a drop at 0.50, 0.57, and 0.67 (32). The verification of our prediction at a χ_{chol} of 0.57 demonstrated that the umbrella model captures the key molecular interactions between cholesterol and phospholipids. (iv) The umbrella model explained the increase in acyl chain order and reduction of membrane permeability by cholesterol. Since cholesterol molecules need to squeeze into the acyl chain region and partially hide under the phospholipid headgroups, it will restrict the motions of acyl chains or even

force the acyl chain to adapt nearly all-trans conformations. The acyl chain order parameter should increase (33, 34), and membrane permeability should decrease (40). Recent molecular dynamics simulations showed that cholesterol molecules are covered by DPPC headgroups in a bilayer, and the conformation of acyl chains next to cholesterol is quite restricted (35–37). (v) The umbrella model explained the so-called “cholesterol condensing effect”. Since cholesterol is partially hidden under the headgroups of phospholipid, the total surface area of the bilayer should be smaller than the sum of the surface area of a pure phospholipid bilayer and the total cross-sectional area of cholesterol (38, 39). (vi) The umbrella model explained the expansion and reorientation of the phospholipid headgroup. As the cholesterol concentration increases, the phospholipid headgroups need to expand and reorient toward the membrane surface to cover more interfacial area per headgroup. This is consistent with earlier findings that PC headgroups become more hydrated when cholesterol is added (41, 42). Molecular dynamics simulations have shown that the PC headgroup–headgroup distance increases and phospholipids in close contact with cholesterol have a slightly larger average area per headgroup and their headgroups are oriented nearly parallel to the membrane surface (35, 43). (vii) The umbrella model pointed out the molecular driving forces of cholesterol superlattices (i.e., cholesterol forms regular, symmetrical, crystal-like, lateral distributions in a fluid lipid bilayer). Cholesterol superlattices have been successfully simulated at cholesterol mole fractions of 0.154, 0.25, 0.40, and 0.5, based on a form of multibody interaction energy derived from the umbrella model (19). (viii) The umbrella model also suggested a possible driven force of lipid raft formation (25). In a lipid mixture with PC having unsaturated chains and sphingolipids having more saturated chains, cholesterol can mix well with both lipids, since both can provide the needed coverage for cholesterol. However, association with sphingolipids can be much more favorable than association with PCs, because the unfavorable chain entropy effect will be reduced by the long and saturated sphingolipid hydrocarbon chains having a natural tendency to form straight conformations. This explanation is consistent with the experimental findings that cholesterol has a low affinity for unsaturated acyl chains and can selectively associate with saturated chains even in a pure PC bilayer (44, 45). On the basis of our Monte Carlo simulation (19), this entropy effect can be quite large. Thus, it is likely to be the driving force of lipid raft formation. In addition, the same argument explains why ceramide also has a strong tendency to partition into lipid raft domains (14). (ix) In this study, the COD reaction rate data validated our previous prediction that the chemical potential of cholesterol must increase sharply as the cholesterol mole fraction approaches its maximum solubility in a bilayer (18). In addition, the high affinity of ceramide for PC bilayers and the 1:1 displacement of cholesterol by ceramide are explained well by the umbrella model. In summary, the umbrella model describes the important molecular interactions between membrane molecules with small polar headgroups (such as cholesterol, ceramide, and diacylglycerides) and membrane molecules with large polar headgroups (such as PC and sphingomyelins). These interactions play key roles in regulating physical and chemical properties of membranes, determining the maximum solubility of ceramide and cho-

lesterol, formation of the cholesterol regular distributions, formation of the raft domains, and the preferential association of lipid molecules within the bilayers.

ACKNOWLEDGMENT

We thank Prof. Jeffrey T. Buboltz of Colgate University (Hamilton, NY) for helping with the RSE method.

REFERENCES

- Field, K. A., Holowka, D., and Baird, B. (1997) Compartmentalized activation of the high affinity immunoglobulin E receptor within membrane domains, *J. Biol. Chem.* **272**, 4276–4280.
- Brown, D. A., and London, E. (1998) Functions of lipid rafts in biological membranes, *Annu. Rev. Cell Dev. Biol.* **14**, 111–136.
- Simons, K., and Ikonen, E. (2000) How cells handle cholesterol, *Science* **290**, 1721–1726.
- Michell, R. H., and Wakelam, M. J. O. (1994) Second messengers: Sphingolipid signaling, *Curr. Biol.* **4**, 370–373.
- Hannun, Y. A. (1996) Functions of ceramide in coordinating cellular responses to stress, *Science* **274**, 1855–1859.
- Ruvolo, P. P. (2003) Intracellular signal transduction pathways activated by ceramide and its metabolites, *Pharmacol. Res.* **47**, 383–392.
- Michael, J. M., Lavin, M. F., and Watters, D. J. (1997) Resistance to radiation-induced apoptosis in Burkitt's lymphoma cells is associated with defective ceramide signaling, *Cancer Res.* **57**, 3600–3605.
- van Blitterswijk, W. J., van der Luit, A. H., Veldman, R. J., Verheij, M., and Borst, J. (2003) Ceramide: Second messenger or modulator of membrane structure and dynamics? *Biochem. J.* **369**, 199–211.
- Luberto, C., and Hannun, Y. A. (2000) Use of short-chain ceramides, *Methods Enzymol.* **312**, 407–420.
- Bose, R., Verheij, M., Haimovitz-Friedman, A., Scotto, K., Fuks, Z., and Kolesnick, R. (1995) Ceramide synthase mediates daunorubicin-induced apoptosis: An alternative mechanism for generating death signals, *Cell* **82**, 405–414.
- Massey, J. B. (2001) Interaction of ceramides with phosphatidylcholine, sphingomyelin and sphingomyelin/cholesterol bilayers, *Biochim. Biophys. Acta* **1510**, 167–184.
- Scheffer, L., Solomonov, I., Weygand, M. J., Kjaer, K., Leiserowitz, L., and Addadi, L. (2005) Structure of cholesterol/ceramide monolayer mixtures: Implications to the molecular organization of lipid rafts, *Biophys. J.* **88**, 3381–3391.
- Ohta, N., and Hatta, I. (2002) Interaction among molecules in mixtures of ceramide/stearic acid, ceramide/cholesterol and ceramide/stearic acid/cholesterol, *Chem. Phys. Lipids* **115**, 93–105.
- London, M., and London, E. (2004) Ceramide selectively displaces cholesterol from ordered lipid domains (rafts): Implications for lipid raft structure and function, *J. Biol. Chem.* **279**, 9997–10004.
- Yu, C., Alterman, M., and Dobrowsky, R. T. (2005) Ceramide displaces cholesterol from lipid rafts and decreases the association of the cholesterol binding protein caveolin-1, *J. Lipid Res.* **46**, 1678–1691.
- Nybond, S., Bjorkqvist, Y. J., Ramstedt, B., and Slotte, J. P. (2005) Acyl chain length affects ceramide action on sterol/sphingomyelin-rich domains, *Biochim. Biophys. Acta* **1718**, 61–66.
- Huang, J., Buboltz, J. T., and Feigenson, G. W. (1999) Maximum Solubility of Cholesterol in Phosphatidylcholine and Phosphatidylethanolamine Bilayers, *Biochim. Biophys. Acta* **1417**, 89–100.
- Huang, J., and Feigenson, G. W. (1999) A Microscopic Interaction Model of Maximum Solubility of Cholesterol in Lipid Bilayers, *Biophys. J.* **76**, 2142–2157.
- Huang, J. (2002) Exploration of Molecular Interactions in Cholesterol Superlattices: Effect of Multibody Interactions, *Biophys. J.* **83**, 1014–1025.
- Veiga, M. P., Arrondo, J. L. R., Goñi, F. M., and Alonso, A. (1999) Ceramides in phospholipid membranes: Effects on bilayer stability and transition to nonlamellar phase, *Biophys. J.* **76**, 342–350.
- Kingsley, P. B., and Feigenson, G. W. (1979) The synthesis of a perdeuterated phospholipid: 1,2-dimyristoyl-*sn*-glycero-3-phosphocholine-*d*₇₂, *Chem. Phys. Lipids* **24**, 135–147.
- Buboltz, J. T., and Feigenson, G. W. (1999) A Novel Strategy for Preparing Liposomes: Rapid Solvent Exchange, *Biochim. Biophys. Acta* **1417**, 232–245.
- Ahn, K., and Sampson, N. S. (2004) Cholesterol Oxidase Senses Subtle Changes in Lipid Bilayer Structure, *Biochemistry* **43**, 827–836.
- Allain, C. C., Poon, L. S., Chen, C. S., Richmond, W., and Fu, P. C. (1974) Enzymatic determination of total serum cholesterol, *Clin. Chem.* **20**, 470–475.
- Parker, A., Miles, K., Cheng, K. H., and Huang, J. (2004) Lateral distribution of cholesterol in dioleoylphosphatidylcholine lipid bilayers: Cholesterol-phospholipid interactions at high cholesterol limit, *Biophys. J.* **86**, 1532–1544.
- Epand, R. M. (2003) Cholesterol in bilayers of sphingomyelin or dihydrosphingomyelin at concentrations found in ocular lens membranes, *Biophys. J.* **84**, 3102–3110.
- Wang, M. M., Olsher, M., Sugar, I. P., and Parkson, L. C. (2004) Cholesterol superlattice modulates the activity of cholesterol oxidase in lipid membranes, *Biochemistry* **43**, 2159–2166.
- Carrer, D. C., and Maggio, B. (1999) Phase behavior and molecular interactions in mixtures of ceramide with dipalmitoylphosphatidylcholine, *J. Lipid Res.* **40**, 1978–1989.
- Batzri, S., and Korn, E. D. (1973) Single bilayer liposomes prepared without sonication, *Biochim. Biophys. Acta* **298**, 1015–1019.
- Lundberg, B., Lampero, M., and Suominen, L. (1982) Incorporation of cholesterol into serum high and low density lipoproteins, *Chem. Phys. Lipids* **312**, 275–282.
- Brockman, H. L., Momsen, M. M., Brown, R. E., He, L., Chun, J., Byun, H. S., and Bittman, R. (2004) The 4,5-double bond of ceramide regulates its dipole moment, elastic properties, and packing behavior, *Biophys. J.* **87**, 1722–1731.
- Cannon, B., Heath, G., Huang, J., Somerharju, P., Virtanen, J. A., and Cheng, K. H. (2003) Time-resolved fluorescence and Fourier transform infrared spectroscopic investigations of lateral packing defects and superlattice domains in compositionally uniform phosphatidylcholine bilayers, *Biophys. J.* **84**, 3777–3791.
- Stockton, B. W., and Smith, I. C. P. (1976) A deuterium NMR study of the condensing effect of cholesterol on egg phosphatidylcholine bilayer membranes, *Chem. Phys. Lipids* **17**, 251–261.
- Vist, M., and Davis, J. H. (1990) Phase equilibria of cholesterol/dipalmitoylphosphatidylcholine mixtures: ²H nuclear magnetic resonance and differential scanning calorimetry, *Biochemistry* **29**, 451–464.
- Smondryev, A. M., and Berkowitz, M. L. (1999) Structure of dipalmitoylphosphatidylcholine/cholesterol bilayer at low and high cholesterol concentrations: Molecular dynamics simulation, *Biophys. J.* **77**, 2075–2089.
- Tu, K., Klein, M. L., and Tobias, D. J. (1998) Constant-pressure molecular dynamics investigation of cholesterol effects in a dipalmitoylphosphatidylcholine bilayer, *Biophys. J.* **75**, 2147–2156.
- Chiu, S. W., Jakobsson, E., and Scott, H. L. (2001) Combined Monte Carlo and molecular dynamics simulation of hydrated lipid-cholesterol lipid bilayers at low cholesterol concentration, *Biophys. J.* **80**, 1104–1114.
- Leathes, J. B. (1925) Role of fats in vital phenomena, *Lancet* **208**, 853–856.
- Demel, R. A., van Deenen, L. L. M., and Pethica, B. A. (1967) Monolayer interactions of phospholipids and cholesterol, *Biochim. Biophys. Acta* **135**, 11–19.
- Kinsky, S. C., Luse, S. A., Zopf, D., van Deenen, L. L. M., and Haxby, J. (1967) Interaction of filipin and derivatives with erythrocyte membranes and lipid dispersions: Electron microscopic observations, *Biochim. Biophys. Acta* **135**, 844–861.
- Kusumi, A., Subczynski, W. K., Pasenkiewicz-Gierula, M., Hyde, M. J. S., and Merkle, H. (1986) Spin-label studies of phosphatidylcholine-cholesterol membranes: Effects of alkyl chain length and unsaturation in the fluid phase, *Biochim. Biophys. Acta* **854**, 307–317.
- Ho, C., Slater, S. J., and Stubbs, C. D. (1995) Hydration and order of lipid bilayers, *Biochemistry* **34**, 6188–6195.

43. Pasenkiewicz-Gierula, M., Róg, T., Kitamura, K., and Kusumi, A. (2000) Cholesterol effects on the phosphatidylcholine bilayer polar region: A molecular simulation study, *Biophys. J.* 78, 1376–1389.
44. Mitchell, D. C., and Litman, B. J. (1998) Effect of cholesterol on molecular order and dynamics in highly polyunsaturated phospholipid bilayers, *Biophys. J.* 75, 896–908.
45. Niu, S. L., and Litman, B. J. (2002) Determination of membrane cholesterol partition coefficient using a lipid vesicle-cyclodextrin binary system: Effect of phospholipid acyl chain unsaturation and headgroup composition, *Biophys. J.* 83, 3408–3415.

BI060610X